Chapter 6

Current Unbalance and Harmonic Distortion

After the study on the BIPV plants' issues on each single element of the system, let's now consider their impact on the Power Quality (PQ) of the grid-connection. In particular, the consequences on the Power Quality (PQ), with reference to the unbalance and the harmonic distortion, is studied for the case study presented in the first part of this dissertation. At first the PQ indexes defined in the Standards (IEC61000-4-30, IEEE Std 141-1993, IEC61000-4-7, IEC61000-4-30, EN50160, IEEE Std 1459-2010) are used, studying the PQ degradation at low power levels, such as in the morning or in the evening. Thereafter, stressing the point that unbalance of the three-phase currents in a BIPV system may depend on structural aspects of the installation, the effect of partial shading, or both, a number of unbalance indicators are calculated starting from data measured during experimental analyses on a real building-integrated PV system representing different types of unbalance. Detailed information is obtained from indices identifying the balance and unbalance components also in the presence of waveform distortion. These indices extend the current definitions of unbalance given in the power quality standards. The results show that the unbalance cannot be considered negligible even without single-phase inverters and is more significant if non-linear loads add a contribution to both harmonic distortion and unbalance seen from the distribution transformer. The results of the studies presented in

the following are, in part, extracted from [72] for the standard PQ indexes and they are in press [73], at the time of this publishing, for the new PQ indicators.

6.1 Standard PQ indexes for Unbalance and Harmonic distortion

In this section the PQ analysis of the experimental results obtained on the case study BIPV system is exposed. The data have been gathered from the field for a period of one week through a network analyser. The harmonic distortion of phase voltages and currents has been characterized with reference to the generation level. The results show that at low power levels, such as in the morning or in the evening, a PQ degradation is not avoidable, while, at higher output power levels, the presence of the PV system can be beneficial to reduce the harmonic distortion of the phase voltages with respect to the distortion occurring when the PV system is not connected.
Paragraph 6.1.1 illustrates the aspects referring to data logging, measurement and data management. Paragraph 6.1.2 shows and discusses the experimental results obtained for the BIPV system analysed.

6.1.1 Data acquisition and viewing

The measurements have been carried out by using the high-accuracy network analyser Hioki PW3198, during one week in July 2012. The network analyser has eight input channels: four for voltages and four for currents through Rogowsky coils (with minimum sensitivity of 0.1 mV/A for 5000 A full scale) providing voltage signals. The instrument accuracies are for RMS voltage ±0.1% of the range; for RMS current ±1.2% of reading ±0.1% of range with Rogowsky coils; for active power ±1.2% of reading ±0.2% of range with Rogowsky coils. The PW3198 provides a simultaneous digital sampling of voltage and current. The sampling frequency is 200 kHz for measurement of RMS voltage and current, active power and other power values, whereas for harmonic and inter-harmonic analysis the analyser operates with 4096 points, 10 cycles (at 50 Hz) or 4096 points, 80 cycles (at 400 Hz). In normal conditions (with 16 bits of A/D converter resolution)

the maximum voltage is 600 V, and in transient conditions (with A/D converter resolution 12 bits) the maximum peak voltage is 6 kV. The data gathered can be visualized on the network analyser viewer by choosing the variables to be shown. An example in shown in Fig. 6.1, with a first window on the upper part of the screen containing the list of measurements available, a successive window referring to the long-term evolution of a selected quantity in the time domain (e.g., active power), a first window on the lower side of the screen implementing a limit curve (an example is shown for the ITIC curve for voltage dip analysis) to check the effect of events, and the last window showing the voltage and current waveforms in a selected operating point or transient event.

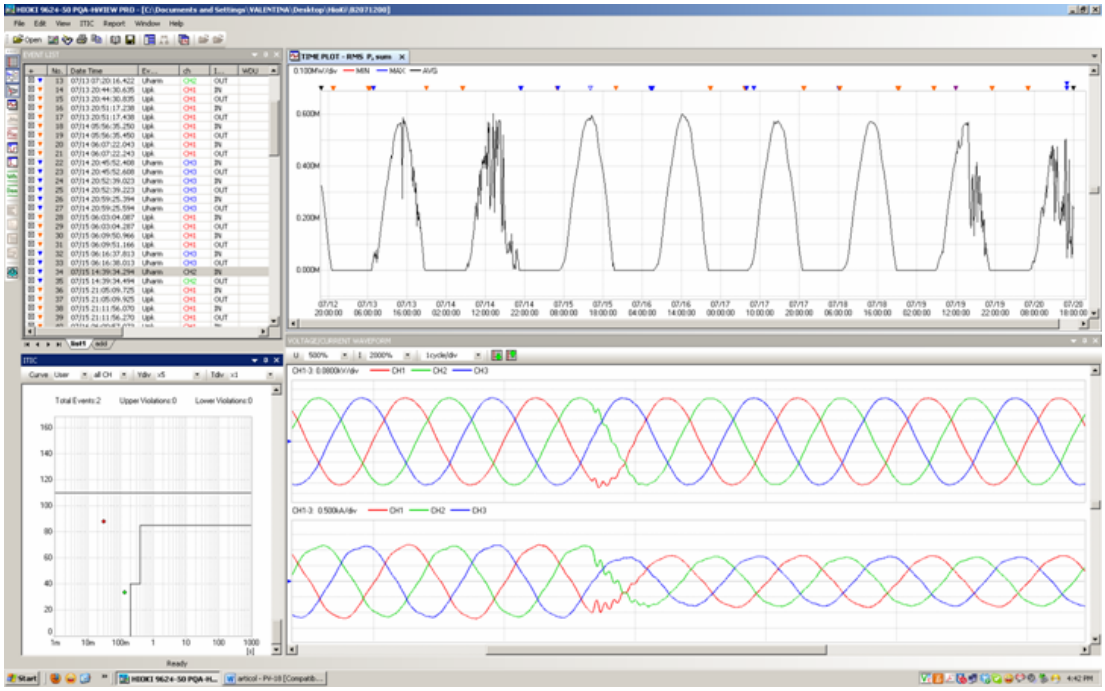

Figure 6.1: The network analyser viewer.

6.1.2 Experimental results

6.1.2.1 Variability of the power generated by the PV system

Fig. 6.1 presents the variation of the active power generated by the BIPV system on the time span of one week. The measurements have been carried out measuring the entire generation from the PV system at the point of common coupling of the grid-connected inverters. The results show that the active power generation follows the evolution of the meteorological conditions. Fig. 6.3 shows the phase voltages and Fig. 6.4 reports the phase currents produced in the three-phase system during the week. The voltage variations are fully acceptable, as the phase voltage oscillates in the range between 238 V and 230 V (all the values belonging to the normal conditions with RMS voltage between 90% and 110% of the rated voltage), while the current depends on the solar irradiance level.

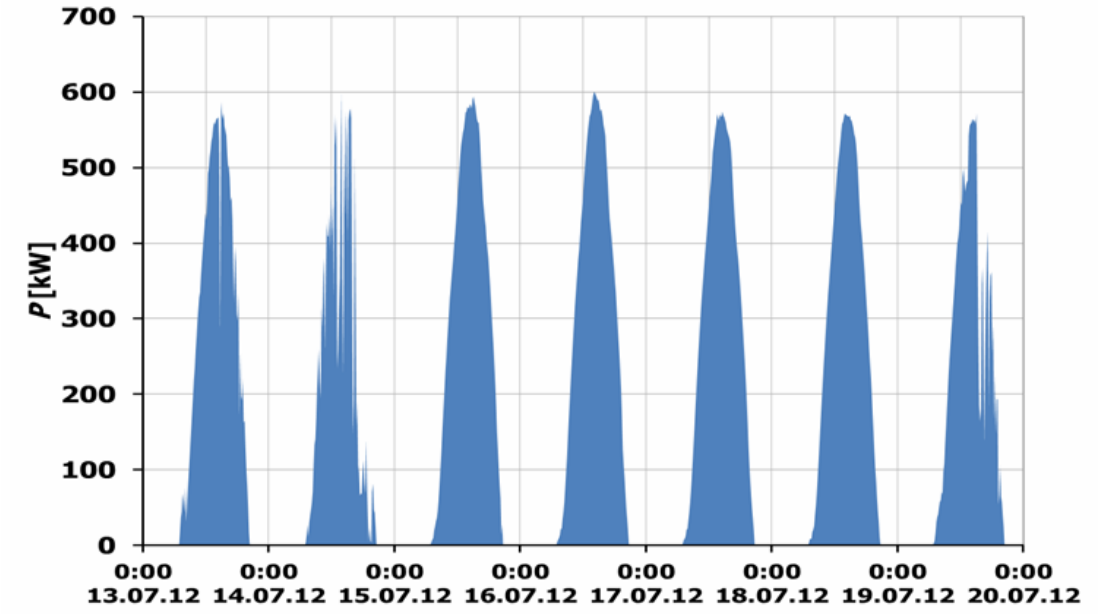

Figure 6.2: Variation of the active power generated from the PV system in one week.

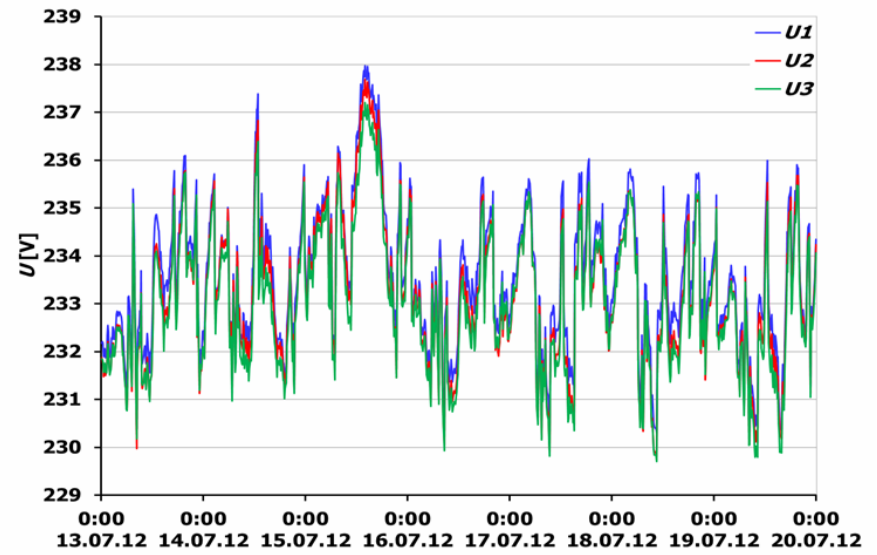

Figure 6.3: Phase voltages at the point of common coupling during the week.

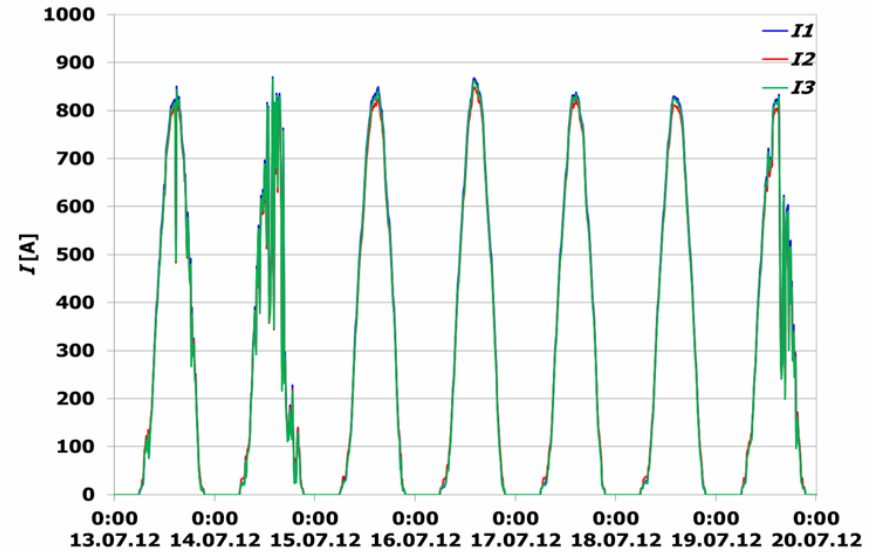

Figure 6.4: Phase currents at the point of common coupling during the week.

6.1.2.2 Assessment of the voltage and current harmonic distortions and unbalance

The harmonics referring to the currents produced by the BIPV system depend on the nature of the source, as well as on the type of inverter technology used for DC/AC conversion and its control strategy. Furthermore, the output current is linked to the harmonics of the voltage at the point of common coupling, which depends on the contribution of all the generations and loads connected to the network. For the BIPV system, a particular aspect referring to the current harmonics is the behaviour of the inverter in conditions of reduced solar irradiance, also due to the effects of shadowing or passing clouds during the day [74]. The following formulas recall the expression of the Standard PQ indexes considered in this section:

$$THD_V = \frac{1}{V_1}\sqrt{\sum_{k=2}^{50} V_k^2} \tag{6.1}$$

$$THD_I = \frac{1}{I_1}\sqrt{\sum_{k=2}^{50} I_k^2} \tag{6.2}$$

$$VUF = \left|\frac{\bar{V}^-}{\bar{V}^+}\right| \tag{6.3}$$

$$CUF = \left|\frac{\bar{I}^-}{\bar{I}^+}\right| \tag{6.4}$$

where

V_1, I_1 are the RMS values of the phase voltage and current at fundamental frequency;

V_k, I_k are the k^{th} harmonic order RMS values of the phase voltage and current;

$\bar{V}^-$, $\bar{V}^+$ are the negative and positive sequence components of phase voltage;

$\bar{I}^-$, $\bar{I}^+$ are the negative and positive sequence components of phase current;

Fig. 6.5 and Fig. 6.6 show the total harmonic distortion THD_V of the phase voltages and THD_I of the phase currents, for different values of the generation level P/P_n. From Fig. 6.5 it is possible to conclude that the THD_V of the

phase voltages in the system analysed remains within acceptable ranges with respect to the limits imposed in the international standards [58]. The THD_I of the phase currents (Fig. 6.6) becomes relatively high only when the generation level is low. For instance, when the generation level is higher than 20% the THD_I never exceeds 10%, while for generation level higher than 60% the THD_I never exceeds the limit 5% valid for rated power conditions according to [60, 75, 76, 77]. Further insights on the evolution of the THD during time can

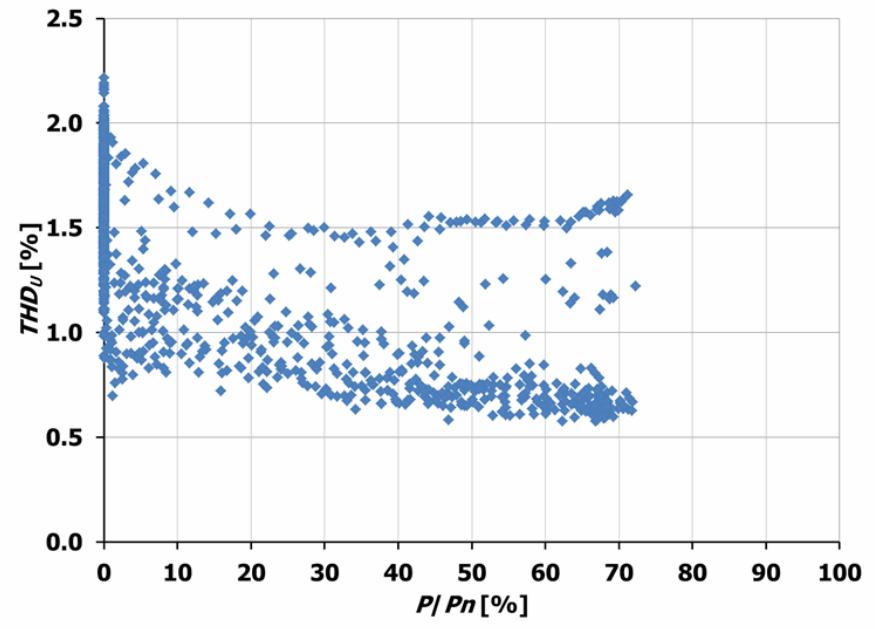

Figure 6.5: Total Harmonic Distortion (THD) of phase voltage in one week.

be obtained by considering the behaviour of the BIPV system in a day with partial clouding conditions and comparing it with its behaviour in a day with clear sky. Fig.s 6.7–6.8 shows the THD_V of the phase voltages. During the night, the PV system is not working and the voltage THD depends on the other components connected to the network, including the local load. During the day, the THD_V decreases significantly. This aspect is an important confirmation of the fact that the grid connection of the PV system is able to improve the power quality characteristics at the point of common coupling, owing to the effect of the inverter control. For instance, the Pulse Width Modulation (PWM) control moves the

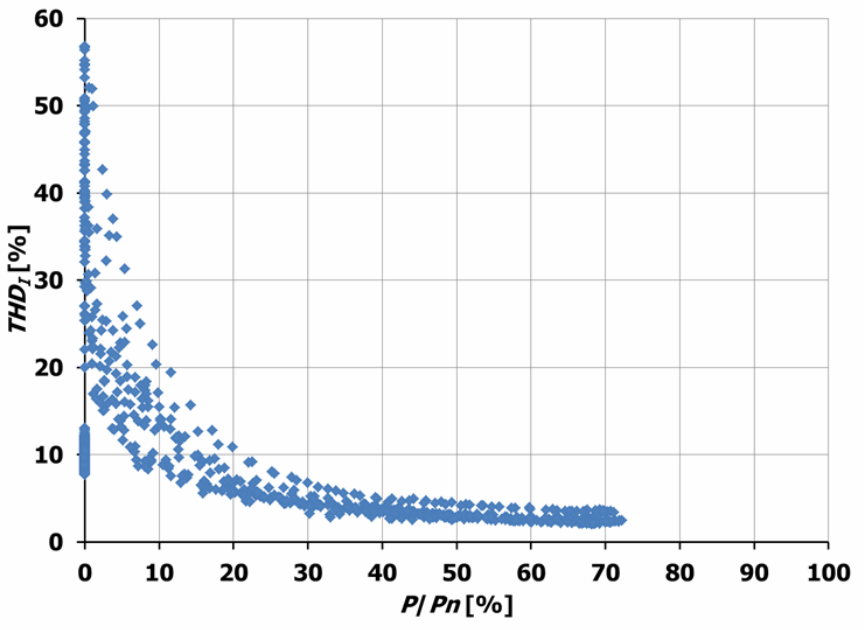

Figure 6.6: Total Harmonic Distortion (THD) of phase current in one week.

harmonic content to relatively high frequencies, that may fall outside the range of frequencies detected when performing harmonic analysis (with harmonic order up to 50). A further confirmation of this fact is that, in general, the improvement in the THD_V values is higher at clear sky with respect to the case with cloudy conditions. Hence, also during the day the THD_V is growing when the impact of the PV system becomes lower and the system is mainly affected by the rest of the grid-connected components. The behaviour of the THD_I of the phase currents during time (Fig.s 6.9–6.10) clearly shows that cases with high values of THD_I are limited to the periods with very small solar irradiance (at the sunset and at the sunrise) and to the effects of passing clouds, while the THD_I is relatively small in conditions with relatively high solar irradiance.

If the attention is focused on a single clear sky day, Fig. 6.11 and Fig. 6.12 represent the evolution of the current and voltage THD and their unbalance factors (CUF, VUF) with respect to the output active power of the whole PV system. Their trends confirm that around the maximum active power level the unbalance and the harmonic distortion are below the technical thresholds [58, 60],

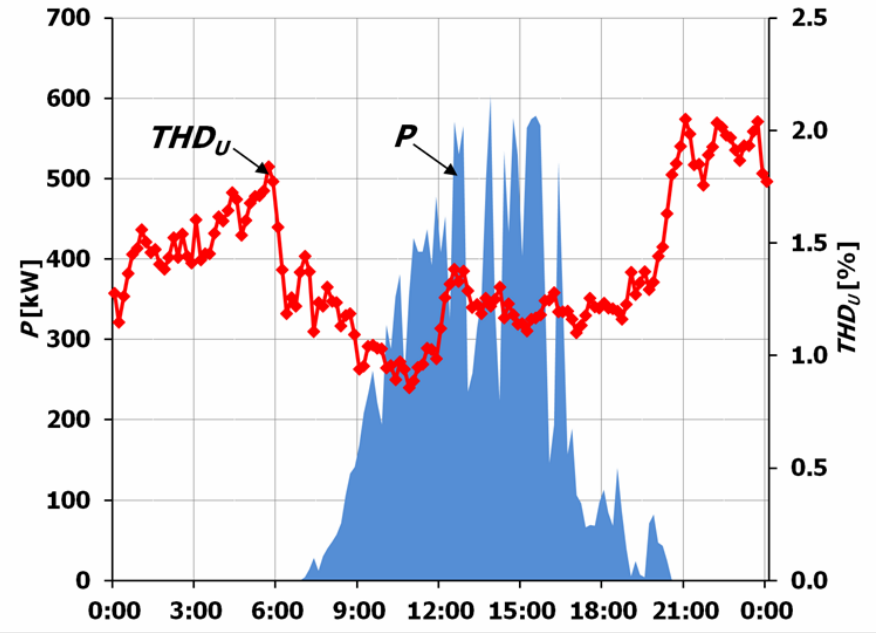

Figure 6.7: Total Harmonic Distortion (THD) of the phase voltage in a day with partial clouding.

since $VUF < 0.2\%$, $CUF < 3\%$, $THD_V < 1\%$ and $THD_I < 5\%$. Conversely, at low power level in the morning and in the evening, the current distortion and unbalance increase, with a slight worsening in the evening compared to the morning. This behaviour has been regularly detected in the tests carried out on the system. Focusing our attention on the current unbalance, this can be caused by the different evolutions of the shade projected by the shed profile over the PV arrays. The uneven exposure to the solar irradiance among the PV arrays and the partial shading of some of them are sources of unbalance. The harmonic distortion is greater in the evening, suggesting that during the last hours of the day the difference in solar irradiance between the exposed and shaded areas is more marked than in the morning. Moreover, the Standard PQ indices do not quantify how much the harmonic distortion does contribute to unbalance, nor to what extent harmonic distortion is affected by the system unbalance. For this reason, other PQ indicators have been taken into consideration in the next section and applied to the output three-phase currents for the study of the current

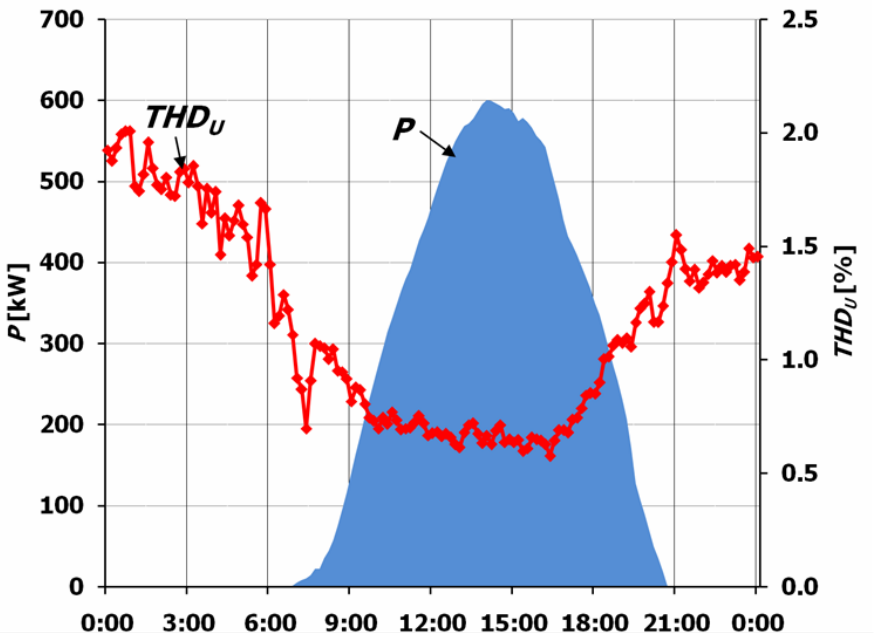

Figure 6.8: Total Harmonic Distortion (THD) of the phase voltage in a clear sky day.

unbalance in BIPV systems.

6.2 Experimental Indicators of Current Unbalance in BIPV Systems

6.2.1 BIPV particularities and typologies of unbalance

After a period of expansion of the installation of grid-connected photovoltaic (PV) systems, mainly ground mounted, in a number of European countries, the recent evolution of the feed-in tariffs, particularly in Italy [78], has brought a sudden decrease in the investments in multi-megawatt Photovoltaic (PV) plants. Thus, the self-consumption of the electrical energy produced by both small (< 20 kW_p) and mid-size (up to 1 MW_p) PV systems, such as those for single family, commercial and industrial users installed in Building Integration (BIPV) is increasing.
Presently, the new policies, aimed at constructing more energy-efficient buildings,

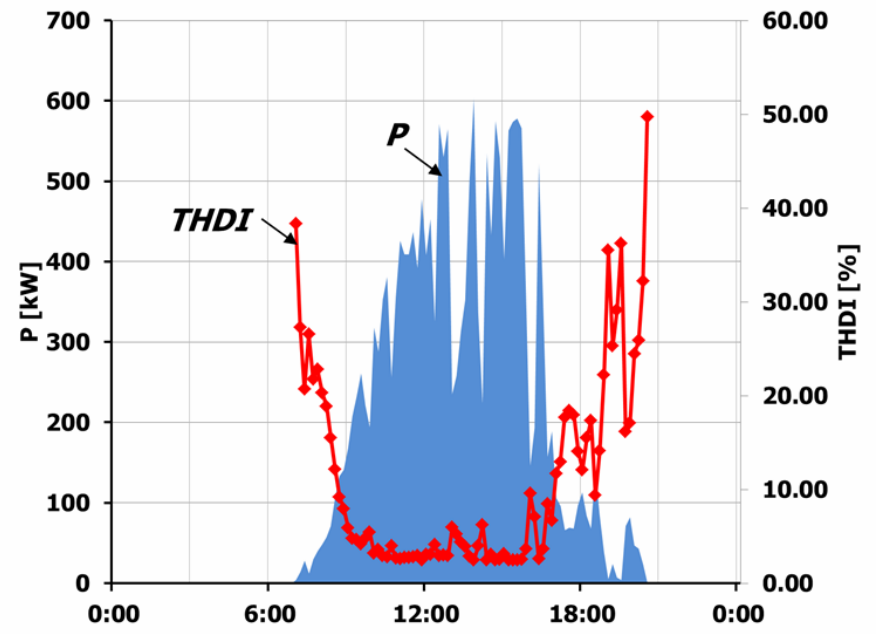

Figure 6.9: Total Harmonic Distortion (THD) of the phase current in a day with partial clouding.

can stimulate the development of Distributed Generation (DG) in the cities. A key issue is the study of the DG impact on the grid, both at Low Voltage (LV) and Medium Voltage (MV) levels, including Power Quality (PQ) aspects [79].
In this new scenario, with a multitude of PV systems operating in a urban environment, the BIPV systems are intrinsically affected by partial shading. Roofs in a city are full of obstacles (e.g., antennas, chimneys, trees, poles, nearby buildings or structures), which are unavoidable for the PV plant installer. Thus, the problem of partial shading over the PV modules can have a high impact on PQ. Moreover, PV plants with a single-phase connection at the LV side of the grid supposedly will be aggregated to each phase of the three-phase Distribution Network (DN). Therefore, it will be difficult to obtain a perfectly balanced configuration. For example, the number of single-phase inverters per each phase may be different or the exposure of the PV arrays to the sun may vary (towards South, East or West).
The focus of this section is to characterize the current unbalance produced by a

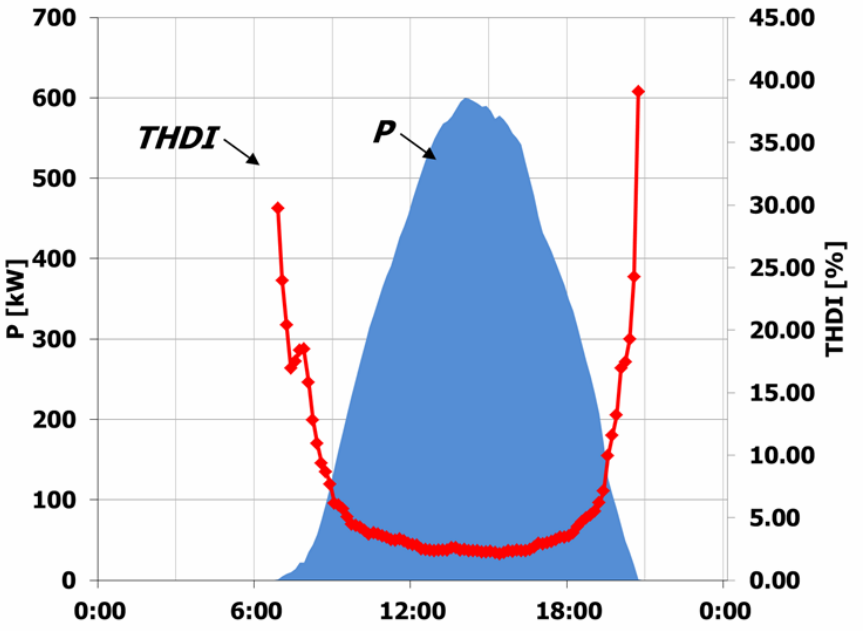

Figure 6.10: Total Harmonic Distortion (THD) of the phase current in a day with partial clouding.

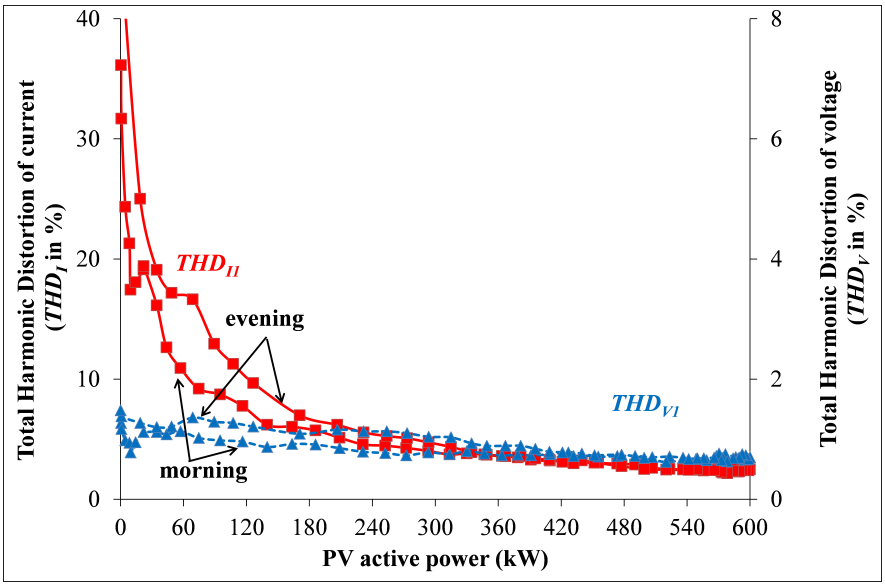

Figure 6.11: Evolution of the THD_I and THD_V for the first phase, during a day in July, in clear sky conditions.

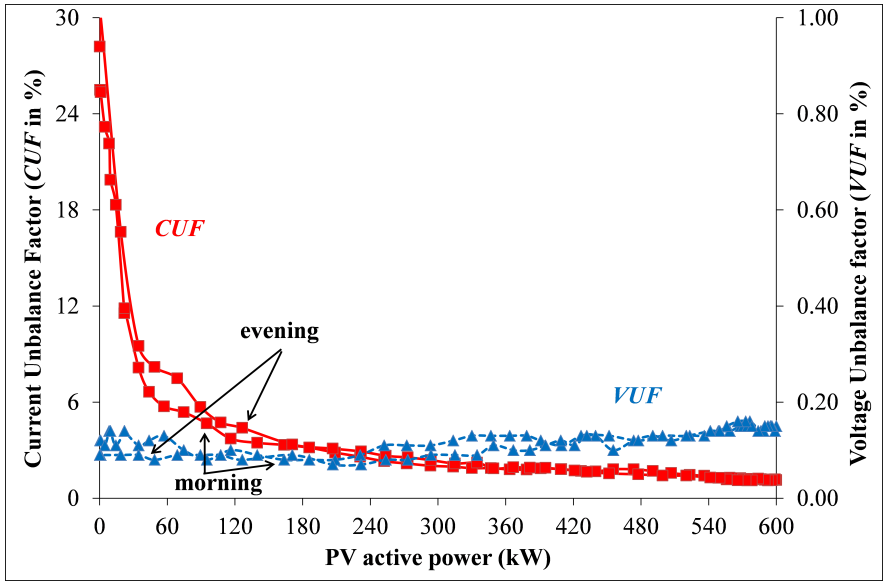

Figure 6.12: Evolution of the Current Unbalance Factor (CUF) and Voltage Unbalance Factor (VUF), during a day in July, in clear sky conditions.

BIPV system connected to the grid, highlighting three typologies of unbalance:

1. "structural unbalance";
2. "unbalance from partial shading";
3. "mixed unbalance".

More emphasis is given to the effect of the partial shading on the PV arrays because this could be the most frequent scenario in practical installations. The case study presented in section 4.3 of this dissertation is analysed, in which all three of the unbalance typologies are observable. Without shading, the possible "structural unbalance" is caused by how the PV field is distributed over the three phases at the PV generator output. Then, two PV arrays with periodic partial shading are studied. Finally, mixed unbalance is considered taking into account also the currents absorbed by the loads (with very different loading in the three phases). Unbalance is analysed using PQ indicators computed by decomposing the three-phase currents with or without the use of the Symmetrical Components (SC) [70]. These indicators are more detailed than those currently adopted

in PQ standards, as they make it possible to determine more accurate values of the unbalance indicators taking into account the harmonic distortion of the waveforms. Paragraph 6.2.2 of this section recalls the unbalance indicators used in PQ analysis. Paragraph 6.2.3 shows and discusses the experimental results. Paragraph 6.2.4 illustrates the suggestions to extend the Unbalance Indicators in PQ Standards. Paragraph 6.2.5 contains the conclusions.

6.2.2 Unbalance Indicators

Various unbalance indicators have been defined for the system voltages and currents. The large majority of the literature studies and standards consider voltage unbalance in three-phase systems, occurring due to unsymmetrical voltage supply among the phases, unsymmetrical line parameters among the phases, or unbalanced loads. One of the effects of unbalance can generally be that the current (and losses) increase in one of the phases, leading the related conductor to reach its temperature limit before the other phases. The classical example on an induction motor associates unbalance with a derating factor (the ratio between the maximum output powers in unbalance and balance conditions), such that no conductor exceeds its thermal limits. A NEMA recommendation [80] indicates a reduction of the induction motor capacity to 75% for a 5% voltage unbalance at fundamental frequency. In [81], three transformer-less photovoltaic inverter topologies for three-phase grid connection are compared also in terms of their effects of unbalance conditions. Structural unbalance between the phases leads to a common-mode voltage component influenced by the difference between the inductors on the phases. In PWM voltage-source converter applications, input-voltage unbalances cause second harmonic voltage components to be injected onto the DC link. The unbalance compensation solution in [82] is designed to minimize the amount of second harmonic regardless of the input voltage unbalance types, using the definitions taken from [83]. Unbalanced voltage variations caused by PV power drop due to moving clouds are analysed in [84] in a small geographic area based on simulations. In [85] a PQ index combines voltage unbalance and harmonic distortions, without measuring individual harmonic distortions in each phase of the power supply. Further authors and documents provide formulations

of the unbalance power. In [86] and [87], instantaneous power flows are analysed for three-phase unbalanced systems with sinusoidal voltages and currents. The instantaneous power approach is applied in [88] to determine the unbalance power from the definition of the IEEE Std. 1459 and from a different expression determined from a study on an unbalanced linear load. For PV generation, a key point is to characterize the current output, as the behaviour of the PV modules is qualitatively close to a current generator (as in the basic PV circuit models with ideal current generator [51] [89]). This point of view makes PV systems relatively different with respect to other plants in which unbalance has been quantified, providing the rationale for studying the unbalance with reference to the system currents. This section recalls a number of unbalance indicators defined in relation to the system phase currents. The unbalance indicators are partitioned into two groups:

1. indicators calculated from variables transformed into symmetrical components;

2. indicators calculated from variables not transformed into symmetrical components.

The transformed current components used to define the indicators are illustrated in the following sub-sections.

6.2.2.1 Current-based components from the SC transformation

For the three phases a, b and c, using the phasor notation, the vector of the complex numbers representing the phase current, at the harmonic order h, is

$$\bar{I}^{(h)} = |\bar{I}_a^{(h)} \bar{I}_b^{(h)} \bar{I}_c^{(h)}| \tag{6.5}$$

Moreover, $\bar{I}_n^{(h)}$ indicates the neutral current phasor. By defining the operator $\alpha = e^{j2\pi/3}$, the SC transformation matrix [70] is denoted as

$$\mathbf{T} = \frac{1}{3} \begin{vmatrix} 1 & \alpha & \alpha^2 \\ 1 & \alpha^2 & \alpha \\ 1 & 1 & 1 \end{vmatrix} \tag{6.6}$$

The matrix $\mathbf{T}$ is directly used in the SCB method [90] to obtain the transformed currents:

$$|\bar{I}_{T_1}^{(h)}\bar{I}_{T_2}^{(h)}\bar{I}_{T_3}^{(h)}|^T = \mathbf{T}\cdot|\bar{I}_{a}^{(h)}\bar{I}_{b}^{(h)}\bar{I}_{c}^{(h)}|^T \tag{6.7}$$

where the subscripts T_1, T_2 and T_3 represent the positive, negative and zero components of the transformed variables, respectively. The rationale of the SCB method is that under balanced conditions the following conditions are verified for m=1, 2, ..., ∞:

1. for h=3m-2, only the positive-sequence component of each h-th harmonic phasor is non-zero;

2. for h=3m-1, only the negative-sequence component of each h-th harmonic phasor is non-zero;

3. for h=3m-3, only the zero-sequence component of each h-th harmonic phasors is non-zero.

In other words, if the three-phase system is balanced the phasors of the harmonic orders 1, 4, 7, ... present only the positive-sequence component, while for the harmonic orders 2, 5, 8, ... there is only the negative-sequence component and for triplen harmonics (i.e., 3, 6, 9, ...) only the zero-sequence component exists. The Euclidean sum of these components can be taken as an index of how balanced the system is. Any unbalance would result in the appearance of positive and/or negative-sequence terms for the various harmonics [91]. Hence, the transformed currents can be used to define the balance phase current component $I_p^{(b)}$, unbalance component $I_p^{(u)}$ and distortion component $I_p^{(u)}$:

$$I_p^{(b)} = \sqrt{\sum_{m=1}^{\infty}\left[\left(I_{T_1}^{(3m-2)}\right)^2+\left(I_{T_2}^{(3m-1)}\right)^2+\left(I_{T_3}^{(3m-3)}\right)^2\right]} \tag{6.8}$$

$$I_p^{(u)} = \sqrt{\sum_{m=1}^{\infty}\left[\begin{array}{lll}\left(I_{T_1}^{(3m-1)}\right)^2+ & \left(I_{T_1}^{(3m-3)}\right)^2+ & \left(I_{T_2}^{(3m-2)}\right)^2+\\ \left(I_{T_2}^{(3m-3)}\right)^2+ & \left(I_{T_3}^{(3m-1)}\right)^2+ & \left(I_{T_3}^{(3m-2)}\right)^2\end{array}\right]} \tag{6.9}$$

$$I_p^{(d)} = \sqrt{\sum_{h=2}^{\infty}\left[\left(I_{T_1}^{(h)}\right)^2+\left(I_{T_2}^{(h)}\right)^2+\left(I_{T_3}^{(h)}\right)^2\right]} \tag{6.10}$$

Furthermore, the balance phase current at fundamental frequency is expressed as

$$I_p^{(b1)} = I_{T_1}^{(1)} \tag{6.11}$$

and the balance phase current distortion component is

$$I_p^{(bd)} = \sqrt{\left(I_p^{(b)}\right)^2 - \left(I_p^{(b1)}\right)^2} \tag{6.12}$$

In the same way, it is possible to separate the fundamental component also for the unbalance component

$$I_p^{(u1)} = \sqrt{\left(I_{T_2}^{(1)}\right)^2 + \left(I_{T_3}^{(1)}\right)^2} \tag{6.13}$$

from the unbalance phase current distortion component

$$I_p^{(ud)} = \sqrt{\left(I_p^{(u)}\right)^2 - \left(I_p^{(u1)}\right)^2} \tag{6.14}$$

Some variants of the transformation matrix have been used in [92]. The three-phase currents are decomposed into three components, called the balance component (I_{bn}), the first unbalance component (I_{fu}) and the second unbalanced component (I_{su}). The matrix $\mathbf{T_1} = \mathbf{T}$ is applied to the harmonics with order h=3n+1 (for an integer number $n \geq$ âĽě0). Two other matrices are defined, namely, the matrix $\mathbf{T_2}$ applied to the harmonics with order h=3n+2, and the matrix C applied to harmonics with order h=3n:

$$\mathbf{T_2} = \frac{1}{3}\begin{vmatrix} 1 & \alpha^2 & \alpha \\ 1 & \alpha & \alpha^2 \\ 1 & 1 & 1 \end{vmatrix} \tag{6.15}$$

$$\mathbf{T_0} = \frac{1}{3}\begin{vmatrix} 1 & 1 & 1 \\ 1 & \frac{-1-\sqrt{3}}{2} & \frac{-1+\sqrt{3}}{2} \\ 1 & \frac{-1+\sqrt{3}}{2} & \frac{-1-\sqrt{3}}{2} \end{vmatrix} \tag{6.16}$$

Considering for each harmonic h the matrix $\mathbf{T_i}$, with i=1,2,0, the transformed currents are [92]:

$$|\bar{I}_{bn}^{(h)}\,\bar{I}_{fu}^{(h)}\,\bar{I}_{su}^{(h)}|^T = \mathbf{T_i}\cdot|\bar{I}_{a}^{(h)}\,\bar{I}_{b}^{(h)}\,\bar{I}_{c}^{(h)}|^T \tag{6.17}$$

These transformed components are used to determine the equivalent RMS value of the three-phase current I_e

$$I_e^2 = I_{bn1}^2 + I_{u1}^2 + I_{bh}^2 + I_{uh}^2 \tag{6.18}$$

where the following terms have been defined:

- Current unbalanced component (first harmonic)

$$I_{u1}^2 = \left(I_{fu}^{(1)}\right)^2 + \left(I_{su}^{(1)}\right)^2 \tag{6.19}$$

- Current balanced harmonic component, associated with the system balance

$$I_{bh}^2 = \sum_{\substack{h=0\\h\neq 1}}^{\infty}\left(I_{bn}^{(h)}\right)^2 \tag{6.20}$$

- Current unbalanced harmonic component, associated with the system unbalance

$$I_{uh}^2 = \sum_{\substack{h=0\\h\neq 1}}^{\infty}\left[\left(I_{fu}^{(h)}\right)^2 + \left(I_{su}^{(h)}\right)^2\right] \tag{6.21}$$

The equivalent current at the first harmonic [93] is:

$$I_{e1}^2 = \sqrt{\left(I_{T_1}^{(1)}\right)^2 + \left(I_{T_2}^{(1)}\right)^2 + \left(I_{T_3}^{(1)}\right)^2} \tag{6.22}$$

6.2.2.2 Current components not transformed into SC

Starting from the RMS three-phase currents, defined as

$$I_i = \sqrt{\sum_{h=0}^{\infty}\left(I_i^{(h)}\right)^2} \tag{6.23}$$

for $i = a, b, c, n$ representing the phase and neutral conductors, the basic notions are as follows:

- the average absolute current:

$$I_{av} = \frac{I_a + I_b + I_c}{3} \tag{6.24}$$

- the minimum and maximum currents:

$$I_{min} = min\{I_a, I_b, I_c\} \tag{6.25}$$
$$I_{max} = max\{I_a, I_b, I_c\} \tag{6.26}$$

- the equivalent three-phase current [94]:

$$I_{eq} = \sqrt{\frac{(I_a^2 + I_b^2 + I_c^2 + I_n^2)}{3}} \tag{6.27}$$

- the current deviations [95]:

$$d_{I_i} = \frac{1}{I_{eq}} \sqrt{|I_i^2 - I_{eq}^2|} \tag{6.28}$$

which measure, for each phase, the difference between the actual waveform and a reference sinusoid whose RMS value is the equivalent three-phase current 6.2.2.2.

6.2.2.3 Definitions of the unbalance indicators

On the basis of the notation introduced above, the unbalance indicators can be formulated as defined in the following sub-paragraphs (a synthesis of the information is shown in Table 6.1).

6.2.2.3.1 Indicators defined from currents transformed into SC The most popular unbalance indicator is the ratio of negative to positive sequence components, determined using the RMS values at the first harmonic, also known

as Current Unbalance Factor (CUF) [83]

$$CUF = \frac{I_{T2}^{(1)}}{I_{T1}^{(1)}} \tag{6.29}$$

A further version of the CUF can be defined by considering the negative and the positive sequence phasors at the first harmonic, obtaining a complex number called Complex Current Unbalance Factor ($\overline{CCUF}$) [96]

$$\overline{CCUF} = \frac{\bar{I}_{T2}^{(1)}}{\bar{I}_{T1}^{(1)}} \tag{6.30}$$

The previous indicators use only the components at the first harmonic. Some extensions characterize the phase current unbalance for distorted waveforms. The Current Unbalance Indicator (CUNB) has been introduced in [93]

$$CUNB = \frac{1}{I_{eq}} \sqrt{I_{eq}^2 - \left(I_{T_1}^{(1)}\right)^2} \tag{6.31}$$

In [92] the indicator of the total current unbalance in the presence of harmonic distortion (ITUD) is defined as

$$ITUD = \sqrt{\frac{I_{u1}^2 - I_{uh}^2}{\left(I_{bn}^{(1)}\right)^2 + I_{bh}^2}} \tag{6.32}$$

The SCB approach, on the other hand, allows the extension of the typical indicators used for the analysis of unbalanced and distorted systems, defining the indicators referring to the balanced phase current component at fundamental frequency (or including the harmonics). In the first group, they are as follows:

- Phase current balanced distortion factor:

$$\varphi_{pI}^{(bd)} = I_p^{(bd)} / I_p^{(b1)} \tag{6.33}$$

- Phase current unbalanced distortion factor:

$$\varphi_{pI}^{(ud)} = I_p^{(ud)} / I_p^{(b1)} \tag{6.34}$$

- Phase current unbalanced factor at fundamental frequency:

$$\varphi_{pI}^{(u1)} = I_p^{(u1)}/I_p^{(b1)} \tag{6.35}$$

- Phase current overall unbalanced factor [97]:

$$\varphi_{pI}^{(u)} = I_p^{(u)}/I_p^{(b1)} \tag{6.36}$$

while the Total Phase Unbalance (TPU) indicator refers to the total balanced phase current component:

$$TPU_I = I_p^{(u)}/I_p^{(b)} \tag{6.37}$$

With no harmonic distortion, the indicator $\varphi_{pI}^{(u)}$ becomes equal to the CUF (a common indicator of system unbalance). Likewise, the TPU_I indicator extends the unbalance indicator in case of distorted currents. In a perfectly balanced system, $\varphi_{pI}^{(bd)}$ becomes the common Total Harmonic Distortion indicator of the current (THD_I).

6.2.2.3.2 Indicators formulated from the currents not transformed into SC This set of indicators is composed of

- Unbalance Indicator (U_I) [83]

$$U_I = \frac{max\left\{|I_{av} - I_{min}|, |I_{max} - I_{av}|\right\}}{I_{av}} \tag{6.38}$$

- Current Unbalance Index (CUI) [95]

$$CUI = \sqrt{\frac{\left(d_{I_a}^2 + d_{I_b}^2 + d_{I_c}^2\right)}{3}} \tag{6.39}$$

- Absolute Current Deviation

$$\delta_{I_i} = \frac{|I_i - I_{av}|}{|I_{av}|} \tag{6.40}$$

for phases i=a, b and c.

The U_I and CUI give total indicators for three-phase systems, allowing for a concise description of the unbalance condition starting from values easily obtainable from a PQ commercial analyser.

Acronym	**Name**	**Meaning**
$\overline{\mathbf{CCUF}}$	Complex Current Unbalance Factor	negative sequence to positive sequence ratio (complex values)
CUF	Current Unbalance Factor	negative sequence to positive sequence ratio (RMS values)
CUI	Current Unbalance Index	Euclidean sum of the square current deviations w.r.t. equivalent current
CUNB	Current Unbalance Indicator	relative variation of squared positive sequence w.r.t. equivalent current
ITUD	Current Total Unbalance with Distortion	obtained from dedicated components defined after the SC transformation
$\mathbf{TPU_I}$	Total Phase Unbalance	total unbalance to total balance phase current component ratio
$\mathbf{U_I}$	Unbalance Indicator	maximum deviation of the RMS phase current w.r.t. average RMS phase current
$\delta_{\mathbf{I_i}}$	Absolute current deviation	relative variation of the RMS current at phase i w.r.t. average RMS phase current
$\varphi^{(\mathbf{u})}_{\mathbf{pI}}, \varphi^{(\mathbf{ud})}_{\mathbf{pI}}$	Phase current unbalance factors	unbalance components to fundamental frequency RMS current ratio

Table 6.1: Summary of the Unbalance Indicators.

6.2.3 Experimental Results

6.2.3.1 Structural Unbalance

In the this paragraph, the PQ analysis is discussed for the whole PV system in high solar irradiance and no-shade condition to verify the reference values of the unbalance indicators due to "structural unbalance". Several sampled 10-cycle waveforms for each line voltage and current of the three-phase output of the whole PV system have been gathered near the transformer. The measurements have been carried out in the afternoon of a day in May, from 4:00 to 4:20 p.m., with high average solar irradiance, slightly above 950 W/m^2. Fig. 6.13 shows the currents measured in the last acquisition, at around 900 W/m^2 of solar irradiance and an active power output almost equal to 60% of the nominal power of all inverters and 40% with respect to the transformer nominal power. This means that the BIPV system, considered nearly at full power, works at less than 60% of its potential, due to its sub-optimal exposure, presence of obstacles and the temperature effects. Moreover, the inverters and the transformer are far away to be fully loaded.

As illustrated in Fig. 6.14, the total three-phase output power is not constant due to unbalance among the phases, with power of phase b smaller than the others (i.e., 3.5 kW or -2% with respect to average active power of the single phases). This "structural unbalance" is not remarkable, since all the currents are generated by three-phase inverters in high solar irradiance conditions. Table 6.2 reports the average values of the indicators computed. The SC current components reveal that the unbalance at the fundamental frequency (from the CUF value) is around 1%. This is confirmed by the $CUNB$, slightly increasing due to waveform distortion. The relatively low weight of the harmonic distortion on the unbalance is confirmed by comparing the values of and , which are 1.6% for the overall factor and only 0.9% if the fundamental frequency is excluded by the evaluation of the unbalance component of the phase current. Moreover, $\varphi_{pI}^{(u)}$ is equal to TPU_I, at least at the third decimal digit, since $I_p^{(b1)}$ is close to $I_p^{(b)}$, just because the harmonic distortion is small. The THD_I values of the phases are estimated with an average of 2.62%, 2.81% and 2.76%, while the value of $\varphi_{pI}^{(bd)}$ is close (2.6%), meaning that the small unbalance has slight influence on the harmonic distortion.

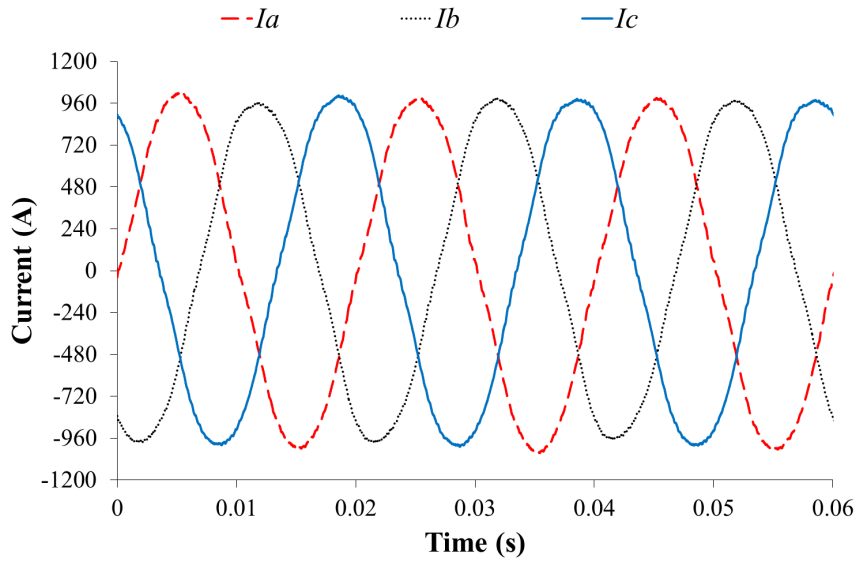

Figure 6.13: Three-phase output currents of the PV system with high solar irradiance (at 16:20 in May 2013).

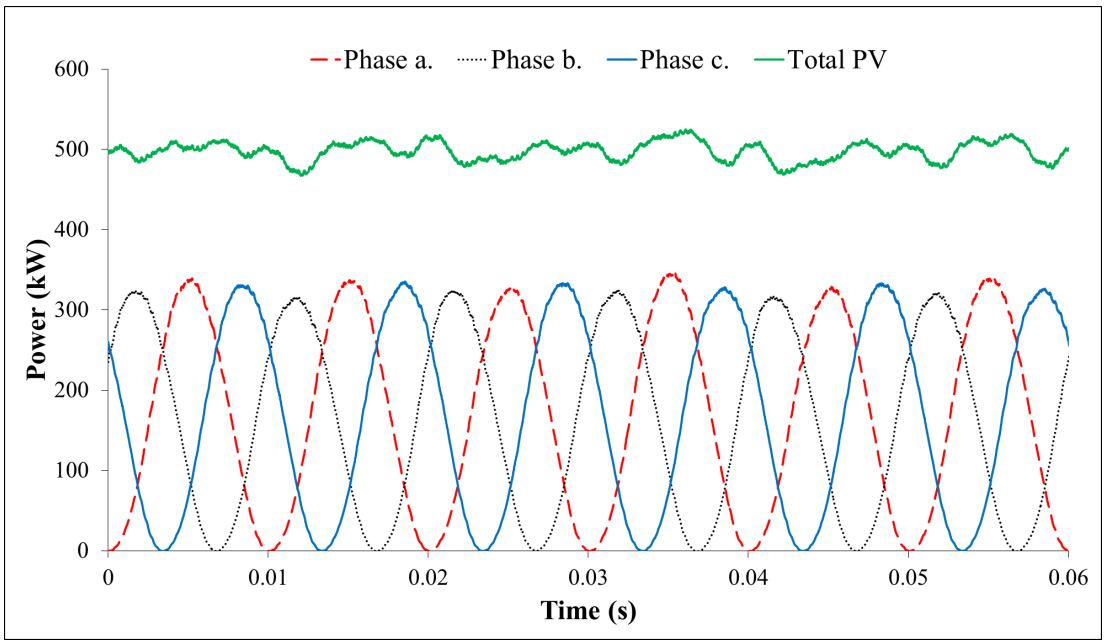

Figure 6.14: Output power for the three phases and the total PV system, with high solar irradiance and no-shading (at hour 16:20 in May 2013).

The alternative current decomposition method tells that the Unbalance Indicator U_I confirms a value around 2%, as well as the Absolute Current Deviations state a disagreement of the RMS values of the phase currents from the value I_{av} of around 1–2%. The Current Unbalance Index (CUI) is 14%, revealing that this indicator gives the highest values. The absolute current deviations allow the identification of the phase that contributes the most to unbalance. The time evolution of the unbalance indicators is almost constant, since the solar irradiance and the shading do not vary very much during the measurements (Fig. 6.15).

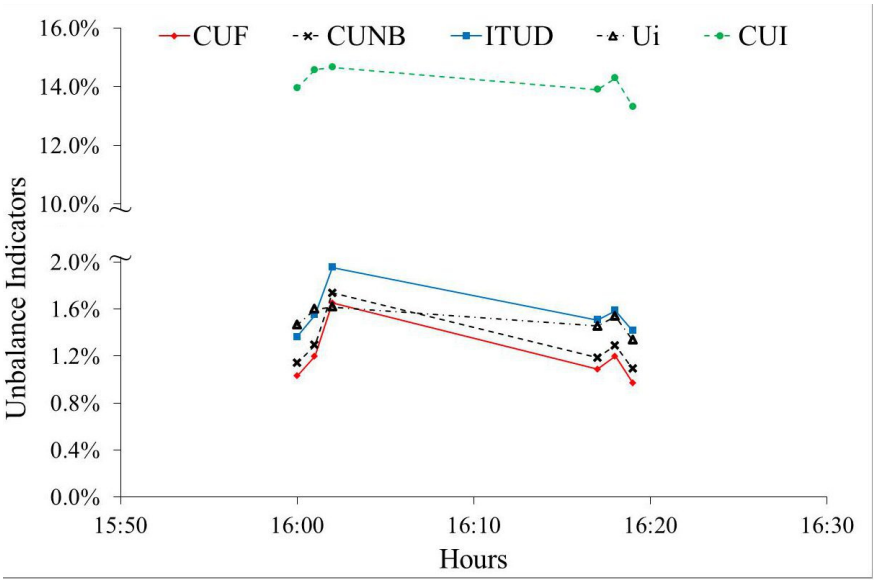

Figure 6.15: Unbalance indicators vs. time in case of structural unbalance. The $ITUD$ and TPU_I values are equal.

6.2.3.2 Unbalance from Partial Shading

The previous paragraph does not highlight the partial shading phenomenon, which affects only some of the PV arrays. The roof of the building is the typical triangular-shape shed and presents tie-beams which strengthen the top structure but create a periodic shading over some PV arrays in the early morning and in the afternoon [56]. The shade evolution causes a diagonal partial shading over the modules, like a series of moving rod-shaped shades. Unbalance is studied for two

Indicators from SC values						
Current component				**Unbalance Indicator**		
$I_p^{(b)}$	[A]	745.69		CUF	[p.u.]	0.012
$I_p^{(b1)}$	[A]	745.43		$\angle CCUF$	[rad]	-0.760
$I_p^{(bd)}$	[A]	19.28		$CUNB$	[p.u.]	0.013
$I_p^{(u)}$	[A]	10.01		$\varphi_{pI}^{(u)}$		0.016
$I_p^{(u1)}$	[A]	8.27		$\varphi_{pI}^{(ud)}$		0.009
$I_p^{(ud)}$	[A]	6.52		TPU_I	[p.u.]	0.016
$I_p^{(d)}$	[A]	20.36		$ITUD$	[p.u.]	0.016
Indicators from non-SC values						
Current component				**Unbalance Indicator**		
I_{eq}	[A]	746.40		U_I	[p.u.]	0.02
d_{I_a}	[p.u.]	0.14		CUI	[p.u.]	0.14
d_{I_b}	[p.u.]	0.18		δ_{I_a}	[p.u.]	0.01
d_{I_c}	[p.u.]	0.11		δ_{I_b}	[p.u.]	0.02
I_a	[A]	753.27		δ_{I_c}	[p.u.]	0.01
I_b	[A]	734.39				.
I_c	[A]	751.10				.
I_{av}	[A]	746.25				.

Table 6.2: Current components and Unbalance Indicators in case of structural unbalance.

arrays of the BIPV system affected by partial shading and their three-phase 100 kVA inverters. The first one (array 5), with a 98 kW_p rated power, is shaded in the morning and, when the measurements were performed in January, the partial shading lasted until the early hours of the afternoon(Fig. 6.16). The partial shading generates a significant distortion in the shape of the I-V curve and makes the Maximum Power Point (MPP) tracker fail, giving variable instantaneous power in the P-V curve (Fig. 6.17) and unbalance in the three-phase current waveforms. Here the MPP tracker (MPPT) is not able to extend the search of the maximum power point up to the global MPP, even if the distances between the global MPP and the operating points of the MPPT are progressively decreasing with the reduction of the shading pattern. The shading pattern involves a few cells in the modules and the bypass diodes, exhibiting the typical changes of slope in P-V curves, work to limit the power losses.

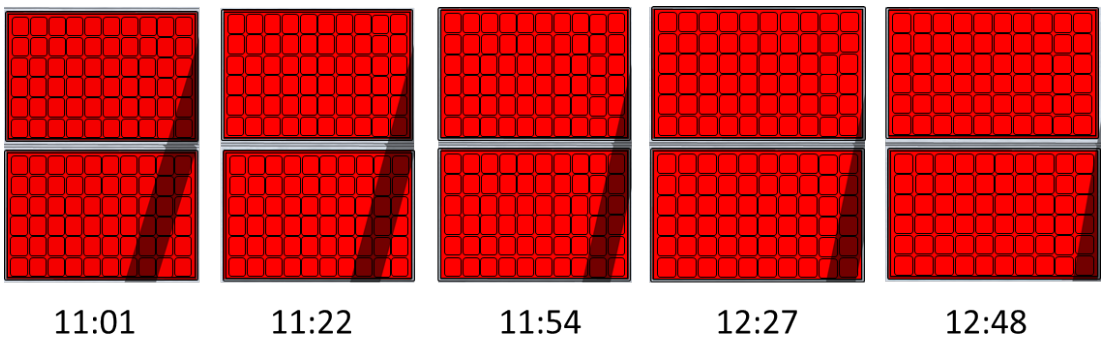

Figure 6.16: Time evolution of the shading over the array no. 5 in the late morning of a day in July 2012 (the hours are indicated under the corresponding pair of PV modules)

Many 10-cycle waveforms have been sampled for each line voltage and current from 12:15 a.m. to 2 p.m.. Fig. 6.18 reports the currents gathered in the last measurement, with average solar irradiance of 354 W/m^2. The output active power is 10% of the inverter nominal power. The second array (array 4), with peak power 98 kW_p, is affected by partial shading in the afternoon. The signal acquisition took place on an April day from 5 to 6 p.m., with average solar irradiance of 560 W/m^2. Again, the output active power is 10% of the inverter

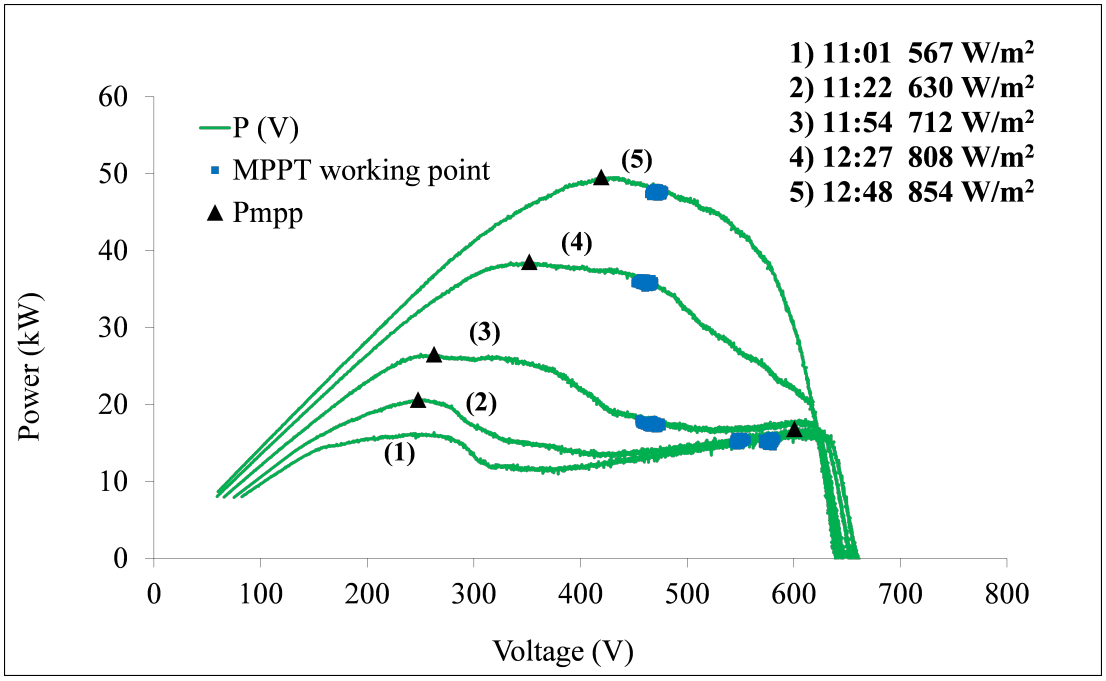

Figure 6.17: Time evolution of the P-V curves over the array no. 5.

nominal power. Table 6.3 and Table 6.4 report the average values of the current components and unbalance indicators for the output currents of both selected three-phase inverters, calculated with the two methods of current decomposition for each measure.

The indicators calculated from SC values reveal that the unbalance at the fundamental frequency is around 11% (CUF). This is confirmed by the $CUNB$, which should take into account the waveform distortion. The harmonic content of the currents is not negligible, as it can be verified by the distortion components $I_p^{(bd)}$ and $I_p^{(ud)}$, whose ratios to the $I_p^{(b1)}$, i.e., $\varphi_{pI}^{(bd)}$ and $\varphi_{pI}^{(ud)}$, are around 16% and 12% respectively for the first inverter and 13% and 11% for the second inverter. These factors are smaller than the THD_I (18%, 23% and 18% in the first case for the three phases and 13%, 17% and 19% in the second case), as shown in the case of structural unbalance, due to the measured unbalance. Therefore, a better evaluation of the impact of the harmonic distortion over the currents' unbalance is given by the TPU_I, around 17% for the first inverter and 15% for the second

Indicators from SC values						
Current component				**Unbalance Indicator**		
$I_p^{(b)}$	[A]	18.82		CUF	[p.u.]	0.107
$I_p^{(b1)}$	[A]	18.68		$\angle CCUF$	[rad]	0.980
$I_p^{(bd)}$	[A]	2.34		$CUNB$	[p.u.]	0.106
$I_p^{(u)}$	[A]	2.84		$\varphi_{pI}^{(u)}$		0.153
$I_p^{(u1)}$	[A]	1.97		$\varphi_{pI}^{(ud)}$		0.109
$I_p^{(ud)}$	[A]	2.02		TPU_I	[p.u.]	0.152
$I_p^{(d)}$	[A]	3.10		$ITUD$	[p.u.]	0.152
Indicators from non-SC values						
Current component				**Unbalance Indicator**		
I_{eq}	[A]	19.91		U_I	[p.u.]	0.09
d_{I_a}	[p.u.]	0.29		CUI	[p.u.]	0.35
d_{I_b}	[p.u.]	0.30		δ_{I_a}	[p.u.]	0.05
d_{I_c}	[p.u.]	0.42		δ_{I_b}	[p.u.]	0.05
I_a	[A]	20.78		δ_{I_c}	[p.u.]	0.09
I_b	[A]	20.80				.
I_c	[A]	18.03				.
I_{av}	[A]	19.87				.

Table 6.3: Current components and Unbalance Indicators in case of partial shading of PV array 4.

Indicators from SC values						
Current component				**Unbalance Indicator**		
$I_p^{(b)}$	[A]	12.08		CUF	[p.u.]	0.113
$I_p^{(b1)}$	[A]	11.92		$\angle CCUF$	[rad]	3.368
$I_p^{(bd)}$	[A]	1.90		$CUNB$	[p.u.]	0.113
$I_p^{(u)}$	[A]	1.98		$\varphi_{pI}^{(u)}$		0.168
$I_p^{(u1)}$	[A]	1.33		$\varphi_{pI}^{(ud)}$		0.122
$I_p^{(ud)}$	[A]	1.45		TPU_I	[p.u.]	0.166
$I_p^{(d)}$	[A]	2.39		$ITUD$	[p.u.]	0.166
Indicators from non-SC values						
Current component				**Unbalance Indicator**		
I_{eq}	[A]	14.61		U_I	[p.u.]	0.10
d_{I_a}	[p.u.]	0.48		CUI	[p.u.]	0.34
d_{I_b}	[p.u.]	0.21		δ_{I_a}	[p.u.]	0.10
d_{I_c}	[p.u.]	0.21		δ_{I_b}	[p.u.]	0.04
I_a	[A]	12.73		δ_{I_c}	[p.u.]	0.06
I_b	[A]	14.67				.
I_c	[A]	14.98				.
I_{av}	[A]	14.13				.

Table 6.4: Current components and Unbalance Indicators in case of partial shading of PV array 5.

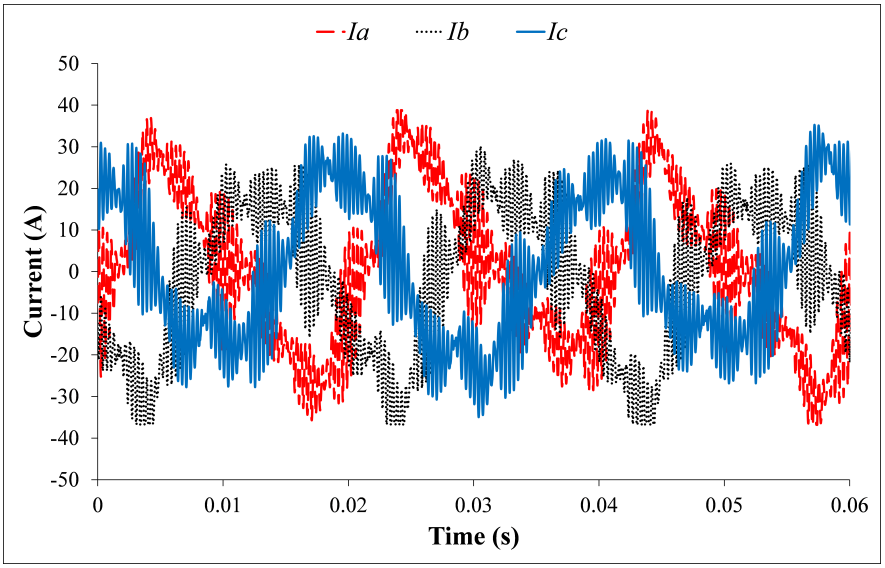

Figure 6.18: Three-phase output currents of the array 5 inverter with partial shading (at 2 p.m. in January 2012).

one (the same values are obtained for the indicator ITUD). The overall unbalance $\varphi_{pI}^{(u)}$ is very close to the TPU_I, but it is slightly greater because $I_p^{(b1)}$ is smaller than $I_p^{(b)}$ due to distortion. From the other set of indicators, the Unbalance Indicator (U_I) confirms a value around 10% for the first inverter and 9% for the second one. The Current Deviations in the first case reveal a disagreement of the RMS values of the phase currents from the equivalent value I_{eq}, which is greater for the phase a and the smallest for phase b. This situation is confirmed also by the Absolute Current Deviations, which considers the average value instead of I_{eq} and gives a value of CUI equal to 34%. In the second case the phases a and b are more aligned, while phase c deviates more from the I_{eq} and I_{av} values. The CUI is very similar as in the first case (35%). In Fig. 6.19 the time evolution of the unbalance indicator for PV array 5 is illustrated as the partial shading decreases. Conversely, the increase of the shading over the PV array 4 is reflected on the slight rise of the unbalance indicators vs. time, as shown in Fig. 6.20.

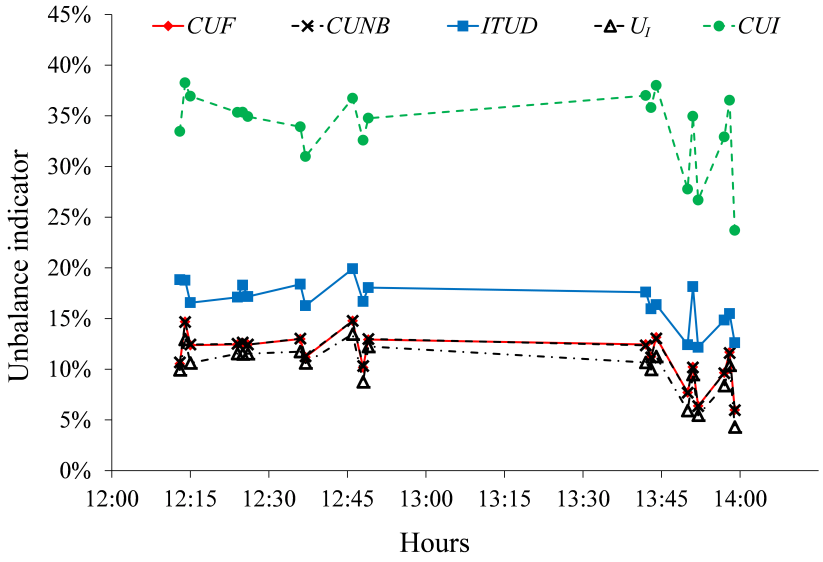

Figure 6.19: Unbalance indicators vs. time with partial shading in the early afternoon (array no. 5). The $ITDU$ and TPU_I values are equal.

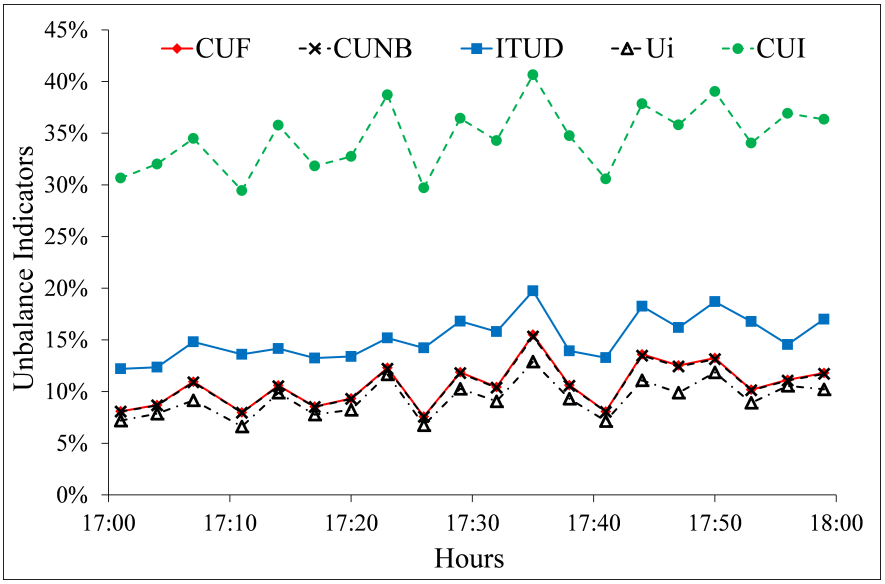

Figure 6.20: Unbalance indicators vs. time with partial shading in the afternoon (array no. 4). The $ITDU$ and TPU_I values are equal.

6.2.3.3 Mixed Unbalance

Finally, the condition of "mixed unbalance" is considered, taking into account the point of common coupling (PCC), where the unbalance is also due to different load currents for each phase absorbed by the internal building services. When the total three-phase currents exchanged with the grid (seen from the distribution transformer) are studied, the situation changes drastically. The signals are gathered from the data acquisition (DAQ) system located just before the transformer around 1:00 p.m. on a June day (Fig. 6.21). During each measurement the general circuit breaker of the PV plant has been opened. Sampling 10 cycles of the waveforms before and after the breaker opening, the total three phase currents exchanged with the grid have been obtained with the PV system connected (Fig. 6.22) and without it (Fig. 6.23). When the circuit breaker is closed, the power injected into the grid is 18% of the inverters' nominal power and 13% of the transformer rated power. The PV generator currents are reconstructed applying the Kirchhoff's law at the current node, making the approximation that the load currents do not change before and after the opening. The overall active power at PV output results around 26% of the inverters' nominal power and 18% of the transformer nominal power. This can be considered an average operating condition of the PV system, i.e., the PV output power is nearly 40% of that with high irradiance. Moreover, this allows us to appreciate the influence of the load currents. When the circuit breaker is open, the loads are absorbing around 8% of the inverter nominal power and 5% of the transformer rated power. The PQ analysis is performed for the total currents exchanged when the breaker is closed. The unbalance indicators (Table 6.5) are very high. The CUF is around 0.36, while TPU_I and $ITUD$ are around 0.38, as for the overall unbalance factor $\varphi_{pI}^{(u)}$. This means that the harmonic distortion has its influence on unbalance. However, this influence is very low compared with the one occurring in case of partial shading. Furthermore, the values of $\varphi_{pI}^{(bd)}$ and $\varphi_{pI}^{(ud)}$ are nearly 0.1, remarkably lower than $\varphi_{pI}^{(u)}$, and $I_p^{(u1)}$ is much greater than $I_p^{(u1)}$; all indicating that the unbalance is mainly due to the component at fundamental frequency. Again, the $\varphi_{pI}^{(bd)}$ is different from the THD_I of each of the three phases (20%, 4% and 7%). The other decomposition method gives an Unbalance Indicator of 30% and a CUI

of 58%. The Current and Absolute Deviations report that the phase b deviates more than the other two phases from the equivalent and average value.

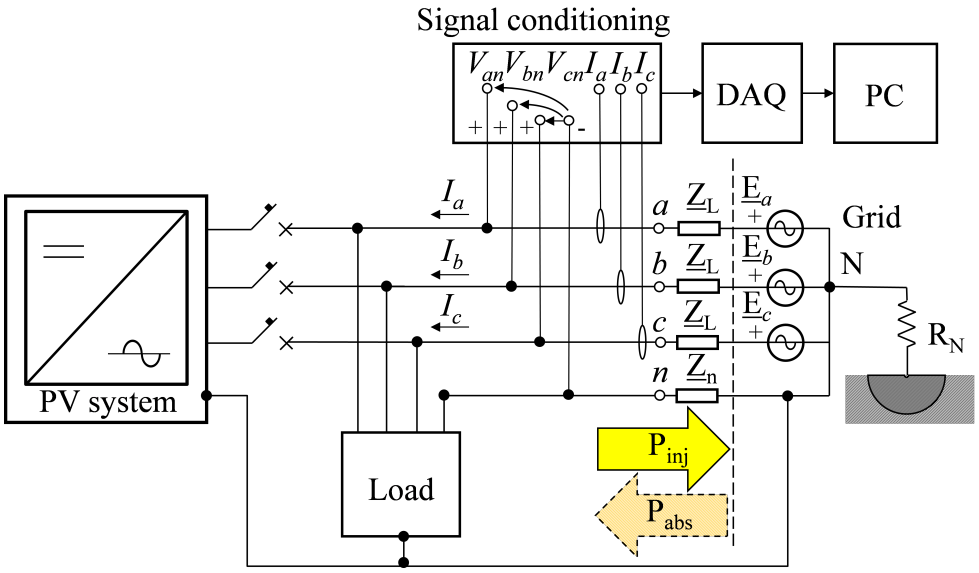

Figure 6.21: Scheme of the three-phase system for signals acquisition.

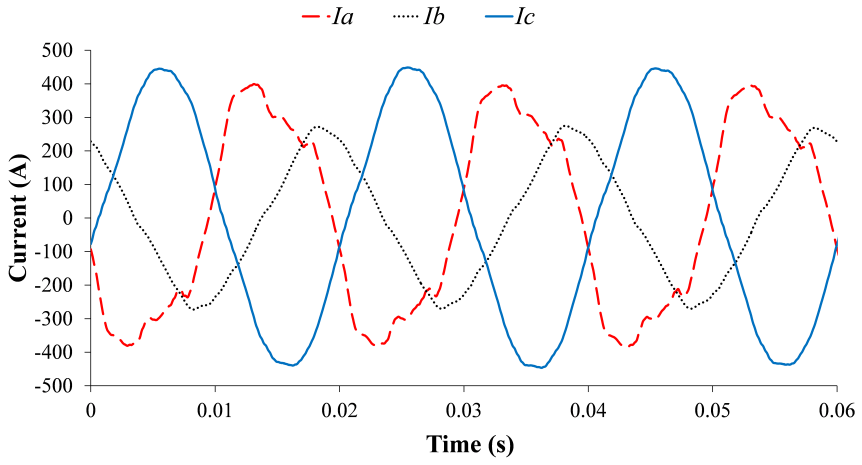

Figure 6.22: Three-phase currents at the PCC with the PV system connected (hour 14:05 in June).

Indicators from SC values						
Current component				**Unbalance Indicator**		
$I_p^{(b)}$	[A]	230.92		CUF	[p.u.]	0.363
$I_p^{(b1)}$	[A]	229.78		$\angle CCUF$	[rad]	-1.518
$I_p^{(bd)}$	[A]	22.86		$CUNB$	[p.u.]	0.344
$I_p^{(u)}$	[A]	86.80		$\varphi_{pI}^{(u)}$		0.378
$I_p^{(u1)}$	[A]	84.04		$\varphi_{pI}^{(ud)}$		0.095
$I_p^{(ud)}$	[A]	21.70		TPU_I	[p.u.]	0.376
$I_p^{(d)}$	[A]	31.52		$ITUD$	[p.u.]	0.376
Indicators from non-SC values						
Current component				**Unbalance Indicator**		
I_{eq}	[A]	250.49		U_I	[p.u.]	0.30
d_{I_a}	[p.u.]	0.30		CUI	[p.u.]	0.58
d_{I_b}	[p.u.]	0.74		δ_{I_a}	[p.u.]	0.09
d_{I_c}	[p.u.]	0.60		δ_{I_b}	[p.u.]	0.30
I_a	[A]	262.00		δ_{I_c}	[p.u.]	0.21
I_b	[A]	167.90				.
I_c	[A]	292.91				.
I_{av}	[A]	240.93				.

Table 6.5: Current components and Unbalance Indicators in case of mixed unbalance.

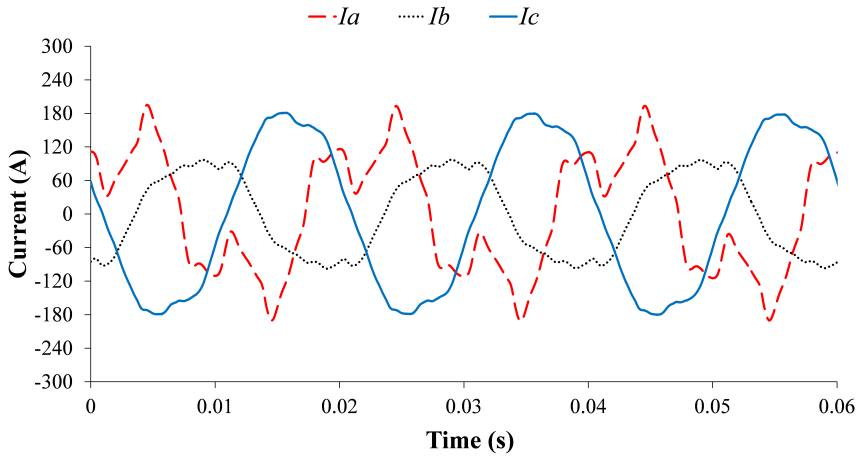

Figure 6.23: Three-phase currents absorbed at the PCC, without PV system (hour 14:05 in June).

6.2.4 Suggestions for extending the Unbalance Indicators in PQ Standards

The results obtained can be useful to promote changes in the current standards in order to account for the dependence of the unbalance components on harmonic distortion in the formulation of the unbalance indicators. On these bases, the values obtained in the application studied can provide some hints. The effectiveness of introducing a new indicator in the standards can be discussed by considering the CUF as the traditional reference. The unbalance indicators TPU_I and $ITUD$ are the most suitable ones, as they can take into proper account the presence of distortion together with unbalance, providing values realistically higher than the CUF in a way depending on harmonic distortion, and becoming equal to the CUF when harmonic distortion is absent. The other indicators may be considered to be less effective. In fact, the values of the $CUNB$ indicator are relatively similar to those of the CUF, and as such could not highlight the effect of harmonic distortion in a sufficient way. Moreover, the CUI and U_I indicators have the potential advantage of being easy to be calculated from the RMS values of the phase and neutral currents, without requiring the symmetrical component transformation. However, in the presence of harmonic distortion the U_I values

could become lower than the traditional CUF values (and as such the U_I could be inappropriate), while the CUI values may be significantly higher than the CUF (even of one order of magnitude, as in Table 6.2) even in the presence of relatively small unbalance, becoming numerically too high with respect to the values traditionally handled by the operators. From the results obtained, a possible limit on TPU_I or $ITUD$ could be indicatively set up to the value 0.1. In this way, it is expected that a PV system with moderate structural unbalance does not exceed the limit, while a PV system subject to consistent partial shading would need some modifications in the placement of the arrays to avoid negative effects on harmonic distortion and unbalance.

6.2.5 Concluding Remarks

The operating conditions of a BIPV systems may lead to the occurrence of different types of unbalance of the currents in the three-phase system. This chapter has proposed a categorization of unbalance into three basic types, with structural unbalance, unbalance from partial shading and mixed unbalance. For each type of unbalance, results from experimental analyses have highlighted that the unbalance in a PV system cannot be considered negligible in the presence of structural issues and can become more relevant with partial shading and unbalanced distorted loads. This aspect is important for designing a PV system and its grid connection, oversizing the distribution transformer if needed. A number of indicators taken from the reviewed literature have been calculated. Some indicators are computed to allow the direct use of the parameters provided by commercial PQ analyzer. The SCB method leads to concise three-phase indicators, making it possible to identify various unbalance components also in the presence of harmonic distortion of the current waveforms. However, in the application considered, the structural, partial shading and mixed unbalance occur within a relatively long time frame with respect to the timing of the measurements, so that the possible saving in computational time is not a crucial aspect. Setting up the limits in the standards is matter of discussion inside the standardization body. According to the present trend of formulation of the standards, the power quality indicators are not assessed individually, but considering the values of the indicator obtained

from a number of successive measurements during a predefined time period and taking for example the 95^{th} percentile (i.e., the 95% non-exceeding probability) from the cumulative distribution of the values of the indicator as the number characterizing the system under test. The acceptability limit is then defined to be applied to the 95% percentile. For PV systems, a key aspect that has to be established refers to the conditions in which the values of the unbalance indicator are considered to be relevant, for example avoiding to compute the indicator with very low solar irradiance, as its value would be poorly meaningful in practice. These aspects are matter for future studies.